American Society of Hematology
2021 L Street NW, Suite 900,
Washington, DC 20036
Phone: 202-776-0544 | Fax 202-776-0545
editorial@hematology.org

# Epigenetic control over cell-intrinsic immune response antagonizes self-renewal in acute myeloid leukemia

Tracking no: BLD-2023-021640R2

Eloisa Felipe Fumero (University of Muenster, Germany) Carolin Walter (Institute of Medical Informatics, University of Muenster, Germany) Joris Frenz (German Cancer Research Center (DKFZ), Germany) Franca Seifert (University Hospital Muenster, Germany) Vijay Alla (University of Münster, Germany) Thorben Hennig (German Cancer Research Center (DKFZ), Germany) Linus Angenendt (University Hospital Münster, Germany) Wolfgang Hartmann (University Hospital Muenster, Germany) Sebastian Wolf (Goethe University Frankfurt, University Hospital, Germany) Hubert Serve (Goethe University Frankfurt, Germany) Thomas Oellerich (Goethe University, Germany) Georg Lenz (University Clinic Münster, Germany) Carsten Müller-Tidow (University Hospital Heidelberg, Germany) Christoph Schliemann (University Hospital Münster, Germany) Otmar Huber (Jena University Hospital, Germany) Martin Dugas (Heidelberg University Hospital, Germany) Matthias Mann (Max-Planck Institute of Biochemistry, Germany) Ashok Kumar Jayavelu (German Cancer Research Center (DKFZ), Germany) Jan-Henrik Mikesch (University Hospital Muenster, Germany) Maria Arteaga (University of Münster, Germany)

**Abstract:**
Epigenetic modulation of the cell-intrinsic immune response holds promise as a therapeutic approach for leukemia. However, current strategies designed for transcriptional activation of endogenous transposons and subsequent interferon type-I (IFN-I) response, show limited clinical efficacy. Histone lysine methylation is an epigenetic signature in IFN-I response associated with suppression of IFN-I and IFN stimulated genes, suggesting histone demethylation as key mechanism of reactivation. In this study, we unveil the histone demethylase PHF8 as a direct initiator and regulator of cell-intrinsic immune response in acute myeloid leukemia (AML). Site-specific phosphorylation of PHF8 orchestrates epigenetic changes that upregulate cytosolic RNA sensors, particularly the TRIM25-RIG-I-IFIT5 axis, thereby triggering the cellular IFN-I response-differentiation-apoptosis network. This signaling cascade largely counteracts differentiation block and growth of human AML cells across various disease subtypes in vitro and in vivo. Through proteome analysis of over 200 primary AML bone marrow samples, we identify a distinct PHF8/IFN-I signature in half of the patient population, without significant associations with known clinically or genetically defined AML subgroups. This profile was absent in healthy CD34-positive hematopoietic progenitor cells, suggesting therapeutic applicability in a large fraction of AML patients. Pharmacological support of PHF8 phosphorylation significantly impairs growth of primary AML patient samples. These findings provide novel opportunities for harnessing the cell-intrinsic immune response in the development of immunotherapeutic strategies against AML.

**Conflict of interest:** No COI declared

**COI notes:**

**Preprint server:** No;

**Author contributions and disclosures:** Conceptualization, J-H.M. and M.F.A.; Methodology, E.F.F., A.K.J., J-H.M. and M.F.A.; Validation, E.F.F., F.S., V.A. and M.F.A.; Formal Analysis, C.W., J.M.F., L.A., M.D., M.M., A.K.J. and M.F.A.; Investigation, E.F.F., F.S., V.A., A.K.J., J-H.M. and M.F.A.; Resources, W.H., S.W., H.S., T.O., G.L., C. M-T., C.S., O.H., M.M., J-H.M. and M.F.A.; Writing-Original Draft, J-H.M. and M.F.A.; Writing-Review & Editing, all authors.; Visualization, J.M.F., T.H., A.K.J. and M.F.A.; Supervision, J-H.M. and M.F.A.; Project Administration, M.F.A., Funding Acquisition, M.F.A.

**Non-author contributions and disclosures:** No;

**Agreement to Share Publication-Related Data and Data Sharing Statement:** Proteomic data sets that were generated during this project are accessible via the Proteomics Identifications Database (PRIDE) • AML cell lines proteome, accession number PXD035635 • Discovery cohort proteome (177 AML patients), accession number PXD023201 Raw and processed genomic data (RNA sequencing and ChIP sequencing) are available with the following accession number GSE211643. Further information and requests for resources and reagents should be directed to and will be fulfilled by the corresponding author, Dr. Maria Francisca Arteaga (marifrancis.arteaga@uni-muenster.de).

**Clinical trial registration information (if any):**

# Epigenetic control over cell-intrinsic immune response antagonizes self-renewal in acute myeloid leukemia

Eloísa Felipe Fumero[1], Carolin Walter[2], Joris Maximillian Frenz[3,4], Franca Seifert[1], Vijay Alla[1], Thorben Henning[3,4], Linus Angenendt[1], Wolfgang Hartmann[5], Sebastian Wolf[6], Hubert Serve[6], Thomas Oellerich[6,7], Georg Lenz[1], Carsten Müller-Tidow[8], Christoph Schliemann[1], Otmar Huber[9], Martin Dugas[10], Matthias Mann[11], Ashok Kumar Jayavelu[3,4,†], Jan-Henrik Mikesch[1,†] and Maria Francisca Arteaga[1, †,*]

[1] Department of Medicine A, University Hospital Muenster, 48149 Muenster, Germany.

[2] Institute of Medical Informatics, University Hospital Muenster, 48149 Muenster, Germany.

[3] Proteomics and Cancer Cell Signaling Group, German Cancer Research Center (DKFZ), Heidelberg, Germany

[4] Department of Pediatric Oncology, Hematology and Immunology, Hopp Children's Cancer Center (KiTZ), University of Heidelberg, Germany.

[5] Division of Translational Pathology, Gerhard-Domagk-Institute for Pathology, University Hospital Muenster, 48149 Muenster, Germany.

[6] Department of Hematology/Oncology, Johann Wolfgang Goethe University, Frankfurt, Germany.

[7] Frankfurt Cancer Institute, Goethe University Frankfurt, Frankfurt, Germany.

[8] Department of Medicine V, University Hospital Heidelberg, Heidelberg, Germany.

[9] Department of Biochemistry II, University Hospital Jena, Friedrich Schiller University Jena, Nonnenplan 2-4, 07743 Jena, Germany.

[10] Institute of Medical Informatics, University Hospital Heidelberg, Heidelberg, Germany.

[11] Department of Proteomics and Signal Transduction, Max Planck Institute of Biochemistry, Martinsried, Germany.

[†] A.K.J., J-H.M. and M.F.A., are co–senior authors and jointly supervised this work.

* Corresponding Author: M.F.A., Department of Medicine A, University Hospital Muenster, Albert-Schweitzer-Campus 1, 48149 Muenster, Germany. E-mail: marifrancis.arteaga@uni-muenster.de



## Data and code availability

Proteomic data sets that were generated during this project are accessible via theProteomics Identifications Database (PRIDE)

- AML cell lines proteome, accession number PXD035635
- Discovery cohort proteome (177 AML patients), accession number PXD023201

Raw and processed genomic data (RNA sequencing and ChIP sequencing) are

available with the following accession number GSE211643.

## Key Points

The histone demethylase PHF8 is a master regulator of cell-intrinsic immune response in acute myeloid leukemia.

Pharmacologically induced PHF8 phosphorylation activates RNA sensors triggering IFN-I response and offering potential for AML immunotherapy.


## Abstract

Epigenetic modulation of the cell-intrinsic immune response holds promise as a therapeutic approach for leukemia. However, current strategies designed for transcriptional activation of endogenous transposons and subsequent interferon type-I (IFN-I) response, show limited clinical efficacy. Histone lysine methylation is an epigenetic signature in IFN-I response associated with suppression of IFN-I and IFN stimulated genes, suggesting histone demethylation as key mechanism of reactivation. In this study, we unveil the histone demethylase PHF8 as a direct initiator and regulator of cell-intrinsic immune response in acute myeloid leukemia (AML). Site-specific phosphorylation of PHF8 orchestrates epigenetic changes that upregulate cytosolic RNA sensors, particularly the TRIM25-RIG-I-IFIT5 axis, thereby triggering the cellular IFN-I response-differentiation-apoptosis network. This signaling cascade largely counteracts differentiation block and growth of human AML cells across various disease subtypes *in vitro* and *in vivo*. Through proteome analysis of over 200 primary AML bone marrow samples, we identify a distinct PHF8/IFN-I signature in half of the patient population, without significant associations with known clinically or genetically defined AML subgroups. This profile was absent in healthy CD34-positive hematopoietic progenitor cells, suggesting therapeutic applicability in a large fraction of AML patients. Pharmacological support of PHF8 phosphorylation significantly impairs growth of primary AML patient samples. These findings provide novel opportunities for harnessing the cell-intrinsic immune response in the development of immunotherapeutic strategies against AML.



## Keywords

Cell-intrinsic immune response, Histone demethylation, PHF8, RNA sensors, IFIT5, INF-Type I response, NFKB, Cancer immunotherapy, Acute myeloid Leukemia.

## Introduction

Avoiding immune destruction is a core hallmark of cancer cells [1]. While modern therapies have revolutionized immune-oncology treatments by targeting T-cell inhibitory or activating pathways, the benefits are limited to a minority of patients [2]. Emerging evidence from solid tumors and hematological malignancies suggests that cancer cell-intrinsic genetic and epigenetic alterations affect tumor immune landscapes[3–6]. Therefore, exploiting the reversibility of those epigenetic marks that control cell-intrinsic immune response presents an attractive platform for the development of more tailored cancer immunotherapies. Epigenetic control of the genome operates through a complex network of regulatory layers and interconnections, which actively facilitate modifications in both DNA and histone tails. Histone lysine methylation is an epigenetic signature in IFN-I response associated with suppression of IFN-I and IFN stimulated genes (ISG)[7,8]. Thus, histone demethylation could be a key mechanism to activate cell-intrinsic immune response. The Jumonji C (JmjC) family of histone lysine demethylases (KDMs) are a novel class of epigenetic enzymes[9] that act in the center of cellular differentiation and proliferation[10,11] contributing to both, normal hematopoiesis[12,13] and leukemogenesis. The Jumonji C family member PHF8 (KDM7B) specifically targets those histone lysine methylation marks that have been associated with repression of IFN-I response[7,14,15]. We hypothesized that controlling histone demethylation of these specific marks could potentiate antiviral response unleashing the IFN-I response network against leukemia.

This study uncovers a trigger of cell-intrinsic immune response: phosphorylated PHF8 directly initiates and regulates cell-intrinsic immune response through histone demethylation. PHF8 activates key initiators of innate immune response including IFIT5, leading to NF-κB driven IFN-I response, differentiation, and apoptosis network against acute myeloid leukemia (AML). Proteome analyses of samples of >200 uniformly treated AML patients identifies a distinct PHF8/IFN type-I signature in half the population that is absent in healthy CD34-positive hematopoietic progenitor cells. Thus, our findings provide a novel strategy harnessing cell-intrinsic immune response for cancer immunotherapy.

## Methods

A detailed description of all methods is presented in the supplemental Methods, available in the Blood Website**.**

### Human/patients samples

Pharmacological studies with primary AML patient samples were approved by the ethics committee of the medical faculty of the University of Heidelberg (S-169/2017) before the study began.

Bone marrow biopsies from AML patients for proteomics analyses were obtained and collected pre- and post-treatment. All patients gave informed consent according to the Declaration of Helsinki to participate in the collection of samples. Use of bone marrow aspirates of AML patients and CD34-positive hematopoietic progenitor cells from healthy volunteers was approved by the Ethics Committee of University Hospital Frankfurt (approval No. SHN-12-2016, amend 01 2021 and 02 2022) and the study alliance leukemia (SAL, approval No. EK98032010) [16]

### Cell characterization Assays

Retroviral/lentiviral transduction and transformation assays were performed on primary murine HSPCs, and human AML cell lines (from DSMZ) as previously described [11]. Briefly, after transduction cells were plated in methylcellulose medium supplemented with cytokines and the suitable antibiotics for selection. Colonies were counted and replated every 5-7 days.

Apoptosis analyses were performed with the PE Annexin V Apoptosis Detection Kit (Becton Dickinson), according to the manufacturer's instructions. Flow cytometry was performed on Attune NxT flow cytometer.

### Xenograft transplantation

All *in vivo* studies were performed as described before [11], and approved by the LANUV NRW under the file number 84-02.04.2015.A231. Briefly, NOD/SCID/IL2rγnull (NSG) mice were injected via tail vein injection with 1x10E5 THP1 transduced cells, after five days of antibiotic selection. Prior to transplantation, mice were conditioned with sublethal radiation (2.5 Gy).

## Drugs

OKA (Merck, Cat. No. 495609-25UG). ATRA (Merck, Cat. No. R2625-50mg).

## RNA-sequencing and analyses

Deep sequencing of the RNA libraries (30x10E6 reads per sample) was carried out on the Illumina NextSeq 500 at the Core Facility Genomics at the Medical Faculty of the University of Muenster.

The alignment was conducted with STAR 2.7.0c against the human reference genome hg38 with default parameters. Read counts per gene were counted with the R package bam signals 3.8. DESeq2 was used to identify differentially expressed genes per condition.

## ChIP-sequencing and analyses

Cells were processed as described before [11]. Briefly, AML cells were formaldehyde crosslinked, SDS lysed and sonicated. The size of the DNA fragments was checked on the Agilent 2100 Bioanalyzer before the library preparation. For each ChIP library the NEBNext® Ultra™ II DNA Library Prep Kit and the NEBNext® Multiplex Oligos for Illumina® were used . Deep sequencing was carried out on the Illumina NextSeq 500.

Raw ChIP-seq reads were aligned to the human reference genome hg38 with BWA 0.7.17, and subsequently sorted with SAMtools 1.9. Peaks were identified with MACS2 and default parameters.

## Deep proteome peptide fractionation

Peptides prepared from THP1 cells with PHF8 AA and PHF8 DD were separated into eight fractions each using the high-pH reversed-phase ‘spider fractionator’ as described elsewhere [17].

## Data dependent acquisition proteomics and data analysis

For sample analysis was used a nanoflow HPLC (EASY-nLC1000, Thermo Fisher Scientific) coupled online to an Orbitrap Exploris480 Mass Spectrometer via a nano electrospray ion source. Mass spectra was acquired in a data dependent mode.

MS raw files were processed using Maxquant version 1.5.5.2 supported by Andromeda search engine. The data was searched for proteins and peptides using a

target-decoy approach with a reverse database against Uniprot Human (version 2018) FASTA file with a false discovery rate of less than 1% at the levels of protein and peptide.

### Phosphoproteome and phosphopeptide enrichment

Samples treatment, lysis and digestion were according to the protocol described previously [18,19].

### Data independent acquisition phosphoproteomics and data analysis

For data-independent data acquisition (DIA), the Thermo Xcalibur Qual Browser (4.0.27.19) software was used for the Exploris 480 instrument.

DIA raw files were analyzed using Spectronaut (Biognosys, Cat. No. Sw-3001, version 14) using the default settings for targeted DIA analysis. Direct DIA search utilizing pulser against the human Uniprot reference proteome database (version August 2018, containing 21.039 entries) was used.

### Proteome and phosphoproteome imputation

We performed data imputation using the in-house open-source Perseus environment (version1.5.2.11) and R (version 4.0.2).

Pharmacological studies with primary AML patient samples were approved by the ethics committee of the medical faculty of the University of Heidelberg (S-169/2017) before the study began. Bone marrow biopsies from AML patients for proteomics analyses were obtained and collected pre- and post-treatment. All patients gave informed consent according to the Declaration of Helsinki to participate in the collection of samples. Use of bone marrow aspirates of AML patients and CD34-positive hematopoietic progenitor cells from healthy volunteers was approved by the Ethics Committee of University Hospital Frankfurt (approval No. SHN-12-2016, amend 01 2021 and 02 2022) and the study alliance leukemia (SAL, approval No. EK98032010) All animal studies were approved by the LANUV NRW under the file number 84-02.04.2015.A231.

## Results

### Epigenetic activity of phosphorylated PHF8 counteracts differentiation block via induction of cell-intrinsic immune response in AML.

To investigate the functional significance of the PHF8 histone demethylase activity in leukemogenesis, we co-transduced primary murine hematopoietic stem-progenitor cells (mHSPCs) with typical AML associated oncogenes or oncofusions and either empty vector (Control), PHF8 wild type (wt) or its catalytically inactive JmjC domain point mutant (F279S) that has been discovered in patients with X-linked mental retardation[20,21]. Only expression of PHF8 with intact histone demethylase activity compromised leukemic transformation and increased cellular differentiation of murine primary HSPCs expressing different AML-associated oncofusions or oncogenes (**Figure 1A-B; supplemental Figure 1A-C**). No effect was observed in cells transduced with the MN1 oncogene known to prevent immune response pathway activation[22] or with E2A-HLF, a chimeric oncoprotein in B-cell lymphoblastic leukemia (**Figure 1D; supplemental Figure 1D-E**). Importantly MLL-fusions, RUNX1-RUNX1T1, CDX2 and CBX7 cells co-transduced with PHF8 wild type only formed few small 3rd colonies with diffuse colony morphology (**supplemental Figure 1F**). Additionally, we demonstrated that wt PHF8 significantly reduced clonogenic growth and increased apoptosis of human AML cells (**Figure 1D-E**). NOD-SCID-Gamma (NSG) mice transplanted with human THP1 AML cells ectopically expressing wt PHF8 showed significantly prolonged disease-free survival (DFS) compared to mice transplanted with THP1 cells transduced with F279S or controls (**Figure 1F**). Transcriptomic and proteomic analyses of human THP1 cells under the same three different conditions confirmed that AML cells overexpressing wt PHF8 showed a significantly distinct gene signature (**supplemental Figure 1G-H**). Systematic pathway analyses of differentially expressed proteins among the three groups revealed that AML cells expressing the F279S mutant were enriched in oncogenic signatures, whereas AML cells with wt PHF8 displayed enrichment of signaling associated with viral transcription, viral reproduction, immunogenic cell death pathways and tumor suppression (**Figure 1G**). These data collectively show that PHF8 histone demethylation activity strongly inhibits leukemogenesis and clonogenic growth in a broad subset of different AML subtypes through the induction of differentiation and apoptosis, and potentially associated with antiviral immune response. However, loss of PHF8 did not affect leukemic transformation, colony morphology, or proliferation of mHSPCs co-transduced with AML-associated oncogenes **(Figure 1H; supplemental Figure 1I-K)** or clonogenic growth of human AML cells **(Figure 1I)**. Thus, changes in expression levels alone do not determine

PHF8 function in leukemia, suggesting that post-translational modifications of the protein are required. In fact, we found significantly increased PHF8 phosphorylation levels upon its overexpression in THP1 cells **(Supplemental Figure 1L)**. PHF8 phosphorylation levels affect its functions [23,24] including cellular responses to retinoic acid [11]. Therefore, we conducted a deep phospho-proteome analysis of THP1 AML cells under all-trans retinoic acid (ATRA) treatment. We identified specific phospho-residues with significant increase in phosphorylation levels of endogenous PHF8 under increasing concentrations of ATRA (**Figure 1J**). Most of these residues exhibited further increased phosphorylation upon higher ATRA concentrations. These results indicate that low levels of ATRA are sufficient to trigger site-specific phosphorylation of PHF8.

While ATRA treatment increased PHF8 phosphorylation in AML cells (**Figure 1J**), the potent protein phosphatase inhibitor, okadaic acid (OKA), has been shown to inhibit PHF8 dephosphorylation[11]. We demonstrated that cell lines with comparably high expression of PHF8 were very susceptible to combinatorial treatment with OKA/ATRA, resulting in a significant reduction of colony formation upon low-dose drug exposure. In contrast, KASUMI-1 cells with low PHF8 levels showed only a moderate response, and MOLM-13 cells with undetectable expression of PHF8, were entirely resistant to this therapy (**Figure 1K-L**). Furthermore, KO of PHF8 abolished the sensitivity of AML cells to OKA/ATRA (**Figure 1M; supplemental Figure 1M**), confirming the requirement of PHF8 for AML blockage by this treatment. Thus, the antileukemic activity of PHF8 across different AML subtypes largely depends on its phosphorylation status. Our data strongly suggests that pharmacological induction of phospho-PHF8 is a promising novel approach to overcome ATRA resistance in AML.

## Site specific phosphorylation of PHF8 blocks growth of AML *in vitro* and *in vivo*

Next, using an inducible expression system that mimics constitutively phosphorylated PHF8 (PHF8 DD, F279S DD) or the non-phosphorylated protein (PHF8 AA, F279S AA) [11,23], we demonstrated that only PHF8 DD compromised colony formation of leukemia cells (**Figure 2A; supplemental Figure 2A**). In cells carrying the catalytically inactive PHF8 mutants (F279S AA, F279S DD), the

phosphorylation status did not induce any functional changes (**Figure 2B**). Cells expressing PHF8 DD showed significantly reduced proliferation and increased apoptosis compared to cells expressing PHF8 AA **(Figure 2C-D)**, while there were no changes in total PHF8 protein levels or cell cycle (**supplemental Figure 2B-C**). Moreover, mice transplanted with human AML THP1-PHF8 DD cells showed significantly improved DFS compared to mice transplanted with THP1-PHF8 AA or THP1 control cells (**Figure 2E; supplemental Figure 2D**). Thus, the antileukemic activity of PHF8 critically depends on both, its demethylase activity as well as the phosphorylation status of the protein.

**The histone demethylase activity of phosphorylated PHF8 triggers interferon type-I response mediated apoptosis.**

We further evaluated the molecular mechanisms underlying growth arrest of THP1-PHF8 DD cells via deep-proteome quantification analysis. Principal component analysis (PCA) and heatmap profiling revealed that PHF8 DD cells contrasted significantly from PHF8 AA cells and from samples carrying catalytically deficient PHF8 (F279S). PHF8 DD cells presented a unique cluster dominated by highly expressed proteins (**Figure 3A-B**). Analysis of specific biological features revealed antiviral defense and IFN type-I response as the most predominant pathways activated by PHF8 DD compared to non-phosphorylated PHF8 (PHF8 AA) or the catalytically inactive mutants (F279S DD and F279S AA) that presented common profiles enriched with pathways of low significance (**Figure 3C; supplemental Figure 3A**). Accordingly, network analysis of highly expressed proteins in PHF8 DD cells revealed functionally interconnected clusters related to IFN response, IL-6 production, innate immune response, immune activation, and induction of apoptosis (**Figure 3D; supplemental Figure 3B-C**).

Further peptide fractionation experiments and direct comparison of the proteomes of PHF8 DD and PHF8 AA cells ultimately highlighted the most significantly upregulated proteins (>log 2) in PHF8 DD cells as part of antiviral response, IFN-I response (**Figure 3E**) and related apoptotic processes (**Figure 3F**). Specifically, 80 proteins were directly associated and shared with IFN signaling related apoptotic pathways (**Figure 3G**). Among the most significantly upregulated proteins in PHF8 DD cells were the dsRNA pattern recognition receptors (PRR), PKR (EIF2AK2), RIG-

I (DDX58), MDA5 (IFIH1), and DDX60 as well as members of the IFIT family, MX1, MX2, STAT1, and components of the oligoadenylate synthetase (OAS) family, all of them part of the anti-viral signature via IFN-I responses, and functionally related with induction of apoptosis or differentiation (**Figure 3H; supplemental Figure 3D**)[25]. Consistently, our transcriptome analysis of PHF8 DD versus PHF8 AA cells showed differentially upregulated genes from the apoptotic FADD-caspase-8 signaling pathway that is typically activated upon IFN-I response mediated late apoptosis (**supplemental Figure 3E**) [26,27].

Together, these results consistently demonstrated that the major antileukemic effects of constitutively phosphorylated PHF8 correlate with the same IFN-I response signaling pathways activated during cell-intrinsic immune response and terminate in its associated late apoptosis pathway.

**Epigenetic activity of phospho-PHF8 confers direct activation of key initiators of cell-intrinsic immune response.**

After identification of the unique activated cluster of PHF8 DD cells linked to cell-intrinsic immune response, we aimed to pinpoint its direct targets, specifically initiators of the IFN-I response. To this end, a new set of RNAseq experiments and genome wide chromatin immunoprecipitation followed by deep sequencing (ChIP-seq) were performed to identify genes activated and the genomic sites occupied by PHF8 depending on its phosphorylation status (PHF8 AA vs. PHF8 DD). The profiles of the ChIP-seq tracks showed significantly higher occupancy of PHF8 DD in promoter regions (**Figure 4A**). As a result of the correlation of the most significantly upregulated genes with PHF8 occupancy at the promoter site, 437 genes were identified (**Figure 4B** and **supplemental Table 1**). These genes fell into five functional clusters where transcription and RNA-binding had the highest significance **(Supplemental Figure 4A**). Among the most significantly upregulated genes, sixteen have functions related with induction of cell intrinsic immune response (**Figure 4C**). Network analysis[28] revealed experimental functional interconnection among five of these genes, *cytidine/uridine monophosphate kinase 2* (*CMPK2)*[29]*, interferon-induced protein with tetratricopeptide repeats 5* (*IFIT5)*[30]*, tripartite motif 25 (TRIM25)*[31]*, transporter associated with antigen processing (TAP1)*[32]*,* and *Moloney leukemia virus 10 (MOV10)*[33] (**Figure 4D**). We confirmed PHF8 as common direct

activator of all five genes **(Supplemental Figure 4B)** and showed that phospho-PHF8 is the transcriptional activator of *CMPK2, IFIT5, TRIM25, TAP1, MOV10* by specific demethylation of the H3K9me2 repressive mark in PHF8 DD vs PHF8 AA (**Figure 4E, supplemental Figure 4C**).

Time course experiments comparing gene expression levels of our five targets, after induction of PHF8 AA or PHF8 DD, revealed a significant increase in *CMPK2*, *IFIT5, TRIM25* expression levels at earlier time points only in PHF8 DD cells, while in the same cells, *TAP1* and *MOV10* expression increased slowly and reached their peak much later **(Figure 4F)**. Significantly increased expression of *CMPK2*, *IFIT5* and *TRIM25* occurred earlier than the increased expression of *IFNb*, indicating their role in initiation of cell-intrinsic immune response (**Figure 4F-G**). In fact, IFIT5 is a RNA binding protein that recognizes endogenous RNAs such as 5'triphosphate-RNA, which is also recognized by RIG-I [34,35], a fundamental RNA sensor and initiator of the antiviral response that triggers *IFNb*. Consistently, in cells expressing PHF8 DD, both RNA binding proteins displayed peak expression levels at earlier time points (**Figure 4F-G**). Furthermore, TRIM25, a key activator of RIG-I, was also directly upregulated by PHF8 DD at the same time points **(Figure 4F)**.

The most notable directly upregulated genes within these clusters were *CMPK2* and *IFIT5* (**Figure 4F**). Consistently in THP1 cells, increased phosphorylation of endogenous PHF8 upon OKA/ATRA treatment results in increased expression of *CMPK2* and *IFIT5* (**Figure 4H-I**).

Both, knock-out of CMPK2 or IFIT5 reversed the effect of PHF8 confirming the crucial role of these two genes for PHF8 mediated growth impairment of human AML (**Figure 4J-K; supplemental Figure 4D-F**).

Thus, our comparative multiomics and functional analyses confirmed that phospho-PHF8 directly induces gene expression signatures of functionally interconnected clusters. The most prominently upregulated genes among these clusters were associated with cell-intrinsic immune response, and most eminently *CMPK2* and *IFIT5*.

**Pharmacological support of PHF8 phosphorylation orchestrates cell-intrinsic immune response in human AML.**

Next, we investigated if the cell-intrinsic immune response triggered by PHF8 phosphorylation could be pharmacologically induced in AML cells. We performed a gene set enrichment analysis (GSEA)[36] correlation comparing published transcriptome data of AML cells treated with high ATRA concentration $10^{-6}$ M (THP1-ATRA) [37] and the transcriptome of AML cells carrying our PHF8 phospho mutants. Indeed, the gene signature of THP1-ATRA cells significantly overlapped with THP1-PHF8 DD cells and contrasted with the THP1-PHF8 AA signature (**Figure 5A**). Thus, we wondered whether simultaneous induction of PHF8 and ATRA treatment could enhance AML destruction synergistically. Indeed, increased expression of PHF8 sensitized AML cells to very low concentrations of ATRA ($10^{-8}$ M) (**Figure 5B-C**). Phosphoproteome analysis of AML cells expressing PHF8 under different ATRA concentrations, identified 15 phospho-residues with increased phosphorylation upon ATRA treatment, with a further increase at higher ATRA concentrations (**supplemental Figure 5A**). These results indicate that low levels of ATRA are sufficient to trigger site-specific phosphorylation of PHF8. Thus, these joint forces within the same pathway decisively enhanced the effect resulting in wide elimination of AML cells.

Phosphoproteome analysis of specific biological features, comparing THP1 cells expressing PHF8 (PHF8) or THP1 empty vector control (EV) after twelve hours of exposure to different ATRA concentrations, revealed significantly enriched phosphorylation levels on proteins and specific kinase motifs involved in the IFN-I response pathways (**Figure 5D; supplemental Figure 5B-E**).

IFIT5 not only functions as RNA binding protein, but also as positive regulator of IFN-I response pulsing nuclear factor κB (NF-κB) activation via increase of phosphorylation and activation of IkB kinase (IKK)[38]. Consistently, our comprehensive phosphoproteome analyses demonstrated increased phosphorylation of known IFIT5 targets, TAK1(MAP3K7) at its functionally relevant residue S439, and IKKB (IKBKB) at active residues S672, S679 (**Figure 5E**). Additionally, our data revealed full activation of the pathway downstream of IKK including phosphorylation of NF-κB inhibitor IkB-epsilon at S157 and IkB-beta at S183 as degradation signals (**Figure 5E**).

The phosphoproteome data shows increased phosphorylation of the NF-κB subunit p65 at Ser45, a critical phosphorylation site known to disrupt DNA binding and transcriptional activity[39] **(Figure 5E)**. Additionally, we observed phosphorylation of GSK3ß at Tyr216, which facilitates the phosphorylation and subsequent degradation of NF-κB subunits [40], including Ser903 and Ser907, which prime NFKB1 for SCF complex, a cluster of NF-κB specific proteasome proteins. Notably, the SCF complex, was directly upregulated by phospho-PHF8 (**Figure 5E**). These results suggest an association between ATRA-induced phosphorylation of PHF8 and the degradation of NF-κB.

Time-course experiments showed IFIT5 expression peaking within the first fifteen minutes of ATRA treatment (**Figure 5F**). NF-κB activation analysis revealed increasing nuclear levels of NF-κB subunit p65 reaching a maximum at sixty minutes of ATRA treatment in AML cells with ectopic PHF8 expression. This finding is consistent with the role of IFIT5 in early activation of NF-κB during early IFN-I response. Nuclear NF-κB subunit p65 levels likewise decreased gradually within the next hours and vanished entirely after 12 hours of ATRA treatment (**Figure 5G**). This indicates a tight control of NF-κB activity (expression) in the nucleus in the presence of ATRA and PHF8.

These results emphasize that pharmacological activation of PHF8 phosphorylation triggers early IFIT5 expression, subsequently leading to a cascade of phosphorylation-mediated activation and inhibition of key regulators involved in the IFN response **(Figure 5H)**.

**A distinct PHF8/IFN-I response protein signature is frequent in AML patients and provides novel therapeutic opportunities.**

To consolidate the finding that interferon signaling pathway proteins are regulated by PHF8, we performed unsupervised enrichment analysis of our proteome dataset from bone marrow biopsies of 177 uniformly treated AML patients [16] and from proteome of relapsed AML patients, together n=204 patient samples. This analysis identified two major groups of interferon signaling protein expression patterns (**Figure 6A; supplemental Table 2**). Based on this unbiased grouping of samples we identified a positive correlation of elevated IFN signaling protein cluster sample group associated with significantly higher PHF8 expression levels (**Figure 6A-B**).

Clinical characteristics did not show relevant differences regarding commonly defined AML subtypes (**supplemental Figure 6A**), or survival between the two groups (**supplemental Figure 6B-D**). Principal component analysis showed a clear dichotomization of the AML cohort with significantly higher expression of PHF8 in cluster 2 (**Figure 6C; supplemental Figure 6E**) whereas PCA of CD34-positive hematopoietic progenitor cells from healthy volunteers did not show clustering (**supplemental Figure 6F**). Combined OKA/ATRA treatment increased PHF8 phosphorylation, reducing clonogenic growth in AML patient samples with high PHF8 levels, while single-agent ATRA or OKA had no significant impact. No change in clonogenic growth was observed in samples with low PHF8 levels **(Figure 6D-I)**. Thus, we identified two AML proteome subgroups (high-PHF8/IFN-I and low-PHF8/IFN-I) based on the interferon signaling cluster. Both subtypes account for about half of the AML patient population and reflect specific biological signatures spanning boundaries of common genetic AML subtypes, and most likely also distinct susceptibility to ATRA/phospho-PHF8-based immunotherapeutic approaches.

## Discussion

The reversibility of epigenetic marks that control the cell-intrinsic immune response provides a promising platform for personalized cancer immunotherapies. Our study reveals PHF8 as the first epigenetic regulator driving cell-intrinsic immune response, promoting differentiation and apoptosis in a wide range of AML subtypes. Targeting PHF8 holds therapeutic potential for AML and provides a new direction for the development of epigenetic-based immunotherapies.

Through systematic multi-omics and functional analyses, we reveal that the collaborative effects of catalytic activity and site-specific phosphorylation of PHF8 drive the acute IFN-I response as primary mechanism underlying the antileukemic activity of the protein in AML.

Histone H3K9me2 is an epigenetic signature in IFN response associated with suppression of IFN and IFN stimulated genes (ISG)[7]. Active IFN and ISG promoters exhibit reduced levels of H3K9me2 and enriched H3K4me3 marks [7]. Given its ability to target H3K9me2 and its distinct characteristics, such as a more flexible interdomain structure, PHF8 represents an ideal candidate for activating the IFN

response more efficiently than other KDMs like LSD1 or KDM7A[14,41]. We provide evidence that phospho-PHF8 specifically targets the repressive H3K9me2 mark, leading to the upregulation of IFIT5 and CMPK2.

Our findings shed light on the role of PHF8 in coordinating the RNA sensing machinery for initiation of cell-intrinsic immune response. We observed a concomitant upregulation of IFIT5, RIG-I and TRIM25, following PHF8 phosphorylation. IFIT5 binds to viral RNA and endogenous 5'-phosphate RNAs [34,35], suggesting its involvement in triggering an innate immune reaction upon detection of endogenous RNA molecules. The simultaneous upregulation of RIG-I, a critical sensor for viral RNA also binding 5'-phosphatase RNAs [42], supports the notion of a coordinated response to RNA patterns. Importantly, this observation aligns with previous reports indicating the colocalization of both proteins with mitochondria, where they synergistically interact with MAVS to enhance the antiviral response [30,34]. TRIM25 serves as a RING-finger E3 ubiquitin ligase crucial for the ubiquitination, stabilization, and activation of RIG-I, thereby facilitating the production of interferon-β [31]. All three proteins exhibit upregulation during ATRA-induced cell differentiation [43], strongly implying a synergistic interplay between the effects of ATRA and PHF8 in initiation of the IFN-I response via the TRIM25-RIG-I-IFIT5 axis. Previous studies have emphasized the importance of dsRNA recognition proteins as key inducers of FADD and caspase-8, which are essential initiators of IFN-I-induced apoptosis [26,27]. Our findings provide compelling evidence that phosphorylated PHF8 induces the upregulation of the entire machinery involved in IFN-induced apoptosis and differentiation.

Furthermore, the progressive upregulation of CMPK2, a mitochondrial protein involved in nucleotide metabolism, cellular homeostasis and antiviral response [29,44], following PHF8 phosphorylation suggests its involvement in cellular energetics and metabolism, reflecting a coordinated adaptation of the cell to mounting antiviral responses. Further investigation of the molecular mechanisms underlying the regulation of CMPK2 by PHF8 will yield valuable insights into the intricate network of immune regulatory pathways and their coordinated role in antiviral defense.

We unveil a novel multifunctional role of IFIT5 as a positive regulator of the early IFN-I response. Consistent with its ability to facilitate NF-κB activation through

interactions with IKK and TAK1 [38], we demonstrate increased phosphorylation of active residues in TAK1 and IKK, indicating that IFIT5 effectively enhances IKK phosphorylation. Moreover, we observe temporal regulation of IFIT5 and nuclear NF-κB subunit p65 upon pharmacological induction of PHF8 phosphorylation, suggesting a coordinated control of NF-κB activity in the presence of ATRA and PHF8. These mechanistic insights provide a deeper understanding of the regulatory network underlying NF-κB activation and highlight the interplay between IFIT5, PHF8, and these signaling molecules.

Our study also implicates that phosphorylated PHF8 stimulates NF-κB inhibition and induces its degradation through distinct mechanisms. Specifically, we observe phosphorylation of the NF-κB subunit p65 at Ser45, consistent with previous studies demonstrating its disruptive effect on DNA binding and transcriptional activity[39]. Additionally, we identify phosphorylation events on NFKB1 and GSK3β, contributing to the degradation of NF-κB subunits and their recognition by the SCF complex, a cluster of NF-κB-specific proteasome proteins[45] . These findings emphasize the multifaceted role of PHF8 regulating NF-κB activity and degradation.

Finally, our unsupervised analysis of AML patient proteome data reveals the presence of a PHF8/IFN-I signature in approximately fifty percent of all AML cases. Importantly, this clustering is absent in CD34-positive hematopoietic progenitor cells from healthy volunteers. These findings, combined with the significant response of primary patient cells with high expression of PHF8 to phospho-PHF8/ATRA treatment, suggest susceptibility of a substantial proportion of AML patients to regimens triggering the phospho-PHF8/IFN-I pathway. Our study provides a novel strategy promoting differentiation and apoptosis via induction of cell-intrinsic immune response and holds promise as a targeted approach for future AML therapies.

## Acknowledgements

This work was funded by The Deutsche Forschungsgemeinschaft (DFG) (No. AR 969/2-1). The project was also supported by IZKF Münster (No. Art1/019/18) and Innovative Medizinische Forschung Universität Münster (No. AR 12 13 11). We would like to thank to the MedK program of the Medical Faculty of Münster University for support of Franca Seifert, to Igor Paron and Mario Oroshi, Department of Proteomics and Signal Transduction at the Max Planck Institute for Biochemistry for excellent mass spectrometry & technical support, to Stefan Froehling, Emily Bernstein, Hugh Brady, and Kristian Helin for CDX2, CBX7, E2A-HLF, and PHF8 constructs respectively, and to all members of the Mikesch-Arteaga lab for constructive discussion.

## Author contributions

Conceptualization, J-H.M. and M.F.A.; Methodology, E.F.F., A.K.J., J-H.M. and M.F.A.; Validation, E.F.F., F.S., V.A. and M.F.A.; Formal Analysis, C.W., J.M.F., L.A., M.D., M.M., A.K.J. and M.F.A.; Investigation, E.F.F., F.S., V.A., A.K.J., J-H.M. and M.F.A.; Resources, W.H., S.W., H.S., T.O., G.L., C. M-T., C.S., O.H., M.M., J-H.M. and M.F.A.; Writing-Original Draft, J-H.M. and M.F.A.; Writing-Review & Editing, all authors.; Visualization, J.M.F., T.H., A.K.J. and M.F.A.; Supervision, J-H.M. and M.F.A.; Project Administration, M.F.A., Funding Acquisition, M.F.A.

## Disclosure of Conflicts of Interest

The authors declare no competing interests.

## Correspondence

Further information and requests for resources and reagents should be directed to and will be fulfilled by the corresponding author, Dr. Maria Francisca Arteaga (marifrancis.arteaga@uni-muenster.de).

## References

1. Hanahan D. Hallmarks of Cancer: New Dimensions. *Cancer Discov*. 2022;12(1):31–46.

2. Demaria O, Cornen S, Daëron M, et al. Harnessing innate immunity in cancer therapy. *Nature*. 2019;574(7776):45–56.

3. Wellenstein MD, Visser KE de. Cancer-Cell-Intrinsic Mechanisms Shaping the Tumor Immune Landscape. *Immunity*. 2018;48(3):399–416.

4. Dufva O, Pölönen P, Brück O, et al. Immunogenomic Landscape of Hematological Malignancies. *Cancer Cell*. 2020;38(3):380-399.e13.

5. Tettamanti S, Pievani A, Biondi A, Dotti G, Serafini M. Catch me if you can: how AML and its niche escape immunotherapy. *Leukemia*. 2022;36(1):13–22.

6. Fennell KA, Bell CC, Dawson MA. Epigenetic therapies in acute myeloid leukemia: where to from here? *Blood*. 2019;134(22):1891–1901.

7. Fang TC, Schaefer U, Mecklenbrauker I, et al. Histone H3 lysine 9 di-methylation as an epigenetic signature of the interferon response. *J Exp Medicine*. 2012;209(4):661–669.

8. Asensio-Juan E, Fueyo R, Pappa S, et al. The histone demethylase PHF8 is a molecular safeguard of the IFNγ response. *Nucleic Acids Res*. 2017;45(7):gkw1346.

9. Kooistra SM, Helin K. Molecular mechanisms and potential functions of histone demethylases. *Nat Rev Mol Cell Bio*. 2012;13(5):297–311.

10. Yi J, Shi X, Xuan Z, Wu J. Histone demethylase UTX/KDM6A enhances tumor immune cell recruitment, promotes differentiation and suppresses medulloblastoma. *Cancer Lett*. 2021;499:188–200.

11. Arteaga MF, Mikesch J-H, Qiu J, et al. The Histone Demethylase PHF8 Governs Retinoic Acid Response in Acute Promyelocytic Leukemia. *Cancer Cell*. 2013;23(3):376–389.

12. Cellot S, Hope KJ, Chagraoui J, et al. RNAi screen identifies Jarid1b as a major regulator of mouse HSC activity. *Blood*. 2013;122(9):1545–1555.

13. Agger K, Nishimura K, Miyagi S, et al. The KDM4/JMJD2 histone demethylases are required for hematopoietic stem cell maintenance. *Blood*. 2019;134(14):1154–1158.

14. Horton JR, Upadhyay AK, Qi HH, et al. Enzymatic and structural insights for substrate specificity of a family of jumonji histone lysine demethylases. *Nat Struct Mol Biol*. 2009;17(1):38–43.

15. Fortschegger K, Shiekhattar R. Plant homeodomain fingers form a helping hand for transcription. *Epigenetics*. 2011;6(1):4–8.

16. Jayavelu AK, Wolf S, Buettner F, et al. The proteogenomic subtypes of acute myeloid leukemia. *Cancer Cell*. 2022;40(3):301-317.e12.

17. Kulak NA, Geyer PE, Mann M. Loss-less Nano-fractionator for High Sensitivity, High Coverage Proteomics *. *Mol Cell Proteom Mcp*. 2017;16(4):694–705.

18. Humphrey SJ, Karayel O, James DE, Mann M. High-throughput and high-sensitivity phosphoproteomics with the EasyPhos platform. *Nat Protoc*. 2018;13(9):1897–1916.

19. Jayavelu AK, Schnöder TM, Perner F, et al. Splicing factor YBX1 mediates persistence of JAK2-mutated neoplasms. *Nature*. 2020;588(7836):157–163.

20. Yu L, Wang Y, Huang S, et al. Structural insights into a novel histone demethylase PHF8. *Cell Res*. 2010;20(2):166–173.

21. Fortschegger K, Graaf P de, Outchkourov NS, et al. PHF8 Targets Histone Methylation and RNA Polymerase II To Activate Transcription ▿ †. *Mol Cell Biol*. 2010;30(13):3286–3298.

22. Sharma A, Yun H, Jyotsana N, et al. Constitutive IRF8 expression inhibits AML by activation of repressed immune response signaling. *Leukemia*. 2015;29(1):157–168.

23. Liu W, Tanasa B, Tyurina OV, et al. PHF8 mediates histone H4 lysine 20 demethylation events involved in cell cycle progression. *Nature*. 2010;466(7305):508–512.

24. Feng H, Lu J, Song X, et al. CK2 kinase-mediated PHF8 phosphorylation controls TopBP1 stability to regulate DNA replication. *Nucleic Acids Res*. 2020;48(19):gkaa756-.

25. Schneider WM, Chevillotte MD, Rice CM. Interferon-Stimulated Genes: A Complex Web of Host Defenses. *Annu Rev Immunol*. 2014;32(1):513–545.

26. Chawla-Sarkar M, Lindner DJ, Liu Y-F, et al. Apoptosis and interferons: Role of interferon-stimulated genes as mediators of apoptosis. *Apoptosis*. 2003;8(3):237–249.

27. Clemens MJ. Interferons and Apoptosis. *J Interf Cytokine Res*. 2003;23(6):277–292.

28. Szklarczyk D, Gable AL, Lyon D, et al. STRING v11: protein–protein association networks with increased coverage, supporting functional discovery in genome-wide experimental datasets. *Nucleic Acids Res*. 2018;47(D1):gky1131.

29. El-Diwany R, Soliman M, Sugawara S, et al. CMPK2 and BCL-G are associated with type 1 interferon–induced HIV restriction in humans. *Sci Adv*. 2018;4(8):eaat0843.

30. Zhang B, Liu X, Chen W, Chen L. IFIT5 potentiates anti-viral response through enhancing innate immune signaling pathways. *Acta Bioch Bioph Sin*. 2013;45(10):867–874.

31. Gack MU, Shin YC, Joo C-H, et al. TRIM25 RING-finger E3 ubiquitin ligase is essential for RIG-I-mediated antiviral activity. *Nature*. 2007;446(7138):916–920.

32. Zhao J, Li R, Li Y, et al. Broadly Antiviral Activities of TAP1 through Activating the TBK1-IRF3-Mediated Type I Interferon Production. *Int. J. Mol. Sci.* 2021;22(9):4668.

33. Cuevas RA, Ghosh A, Wallerath C, et al. MOV10 Provides Antiviral Activity against RNA Viruses by Enhancing RIG-I–MAVS-Independent IFN Induction. *J. Immunol.* 2016;196(9):3877–3886.

34. Katibah GE, Lee HJ, Huizar JP, et al. tRNA Binding, Structure, and Localization of the Human Interferon-Induced Protein IFIT5. *Mol Cell*. 2013;49(4):743–750.

35. Abbas YM, Pichlmair A, Górna MW, Superti-Furga G, Nagar B. Structural basis for viral 5′-PPP-RNA recognition by human IFIT proteins. *Nature*. 2013;494(7435):60–64.

36. Subramanian A, Tamayo P, Mootha VK, et al. Gene set enrichment analysis: A knowledge-based approach for interpreting genome-wide expression profiles. *P Natl Acad Sci Usa*. 2005;102(43):15545–15550.

37. Smitheman KN, Severson TM, Rajapurkar SR, et al. Lysine specific demethylase 1 inactivation enhances differentiation and promotes cytotoxic response when combined with all-trans retinoic acid in acute myeloid leukemia across subtypes. *Haematologica*. 2018;104(6):haematol.2018.199190.

38. Zheng C, Zheng Z, Zhang Z, et al. IFIT5 positively regulates NF-κB signaling through synergizing the recruitment of IκB kinase (IKK) to TGF-β-activated kinase 1 (TAK1). *Cell Signal*. 2015;27(12):2343–2354.

39. Lanucara F, Lam C, Mann J, et al. Dynamic phosphorylation of RelA on Ser42 and Ser45 in response to TNFα stimulation regulates DNA binding and transcription. *Open Biol*. 2016;6(7):160055.

40. Christian F, Smith EL, Carmody RJ. The Regulation of NF-κB Subunits by Phosphorylation. *Cells*. 2016;5(1):12.

41. Chaturvedi SS, Ramanan R, Waheed SO, et al. Conformational Dynamics Underlies Different Functions of Human KDM7 Histone Demethylases. *Chem European J*. 2019;25(21):5422–5426.

42. Chen YG, Hur S. Cellular origins of dsRNA, their recognition and consequences. *Nat Rev Mol Cell Bio*. 2022;23(4):286–301.

43. Wu S-F, Xia L, Shi X-D, et al. RIG-I regulates myeloid differentiation by promoting TRIM25-mediated ISGylation. *Proc National Acad Sci*. 2020;117(25):14395–14404.

44. Lai J-H, Wu D-W, Wu C-H, et al. Mitochondrial CMPK2 mediates immunomodulatory and antiviral activities through IFN-dependent and IFN-independent pathways. *Iscience*. 2021;24(6):102498.

45. Skaar JR, Pagan JK, Pagano M. SCF ubiquitin ligase-targeted therapies. *Nat Rev Drug Discov*. 2014;13(12):889–903.

**Figure 1: Epigenetic activity of phosphorylated PHF8 counteracts differentiation block via induction of cell-intrinsic immune response in AML.**

**(A-C)** Bar charts represent colony numbers in a serial replating assay and typical morphology of cells from fourth round of replating; primary murine hematopoietic stem and progenitor cells were co-transduced with the indicated AML oncogenes or oncofusions as well as with wt PHF8 (PHF8), PHF8-F279S (F279S) or empty vector (Control) respectively. Error bars indicate standard deviation of three independent experiments. Significance was tested using Tukey's multiple comparison test (2-way ANOVA, , * $p < 0.04$, **** $p < 0.000$, nonsignificant ns) **(D)** Bar charts depict colony numbers of human AML cells transduced with PHF8 vs F279S vs Control. Error bars indicate standard deviation of at least four independent experiments. Significance was tested using Tukey's multiple comparison test (2-way ANOVA, **** $p < 0.0001$, *** $p < 0.0004$, ** $p < 0.006$ * $p < 0.04$). **(E)** Bar charts represent early apoptosis as percentage of Annexin-V positive cells from flow cytometry analysis. Error bars indicate standard deviation of four independent experiments. Sidak's multiple comparison test (2way ANOVA, **** $p < 0.0001$ each cell group). **(F)** Kaplan-Meier curves for disease-free survival (DFS) of NSG mice (Charles River Laboratories) transplanted with human THP1 cells transduced with indicated constructs (n=10 mice per group). Six- to eight-week-old NSG mice were injected with 1x10E5 cells, after 5 days antibiotic selection, via tail vein injection. Prior to transplantation, mice were conditioned with sublethal radiation (2.5 Gy). Log-rank (Mantel-Cox) Test was used to compare survival curves. **(G)** Pathways enrichment analysis (Fisher's exact test) of control, PHF8, and F279S cells (n=3, biological replicates per group). Significantly regulated proteins were compared to the unchanged proteome in the dataset based on the Gene Ontology, KEGG, and Keyword terms.

**(H)** Bar charts represent colony numbers of primary murine HSPCs co-transduced with MLL-fusions or CDX2 and sgRNAs for specific CRISPR-Cas9 mediated knock out of *PHF8* (sgRNA 1, sgRNA 2) or non-targeting control (Control). Error bars indicate standard deviations of three independent experiments. Significance was tested using Tukey's multiple comparison test (2-way ANOVA, nonsignificant ns) **(I)** Bar charts represent colony numbers of human AML cells transduced with lenti-CRISPRv2 non-targeting (Control) or lenti-CRISPRv2 guide targeting endogenous PHF8 (sgRNA 1 or sgRNA 3). Error bars indicate standard deviations of four

independent experiments. Significance was tested using Tukey's multiple comparison test (2-way ANOVA, nonsignificant ns) Lower panel: immunoblot analyses showing PHF8 levels. **(J)** Profile plot showing significant increases of phosphorylation in human THP1 AML cells at defined phosphosites of endogenous PHF8 upon 12 hours ATRA treatment compared to controls. Each data point is the averaged median of biological quadruplicate of z-scored log 2 phosphosite intensities; significance was tested using multiple sample t-test (oneway ANOVA, Permutation-based FDR <0.05). **(K)** Violin plots depict numbers of colonies of human AML cells treated with 500nM OKA (OKA 20 minutes incubation) or/and ATRA 10E-8 M. Significance was tested using Tukey's multiple comparison test (2-way ANOVA, * $p < 0.05$ **, $p < 0.0085$, ns). **(L)** Immunoblot of endogenous total PHF8 protein levels. **(M)** Western blot analyses (upper panel) of PHF8 levels before and after knocking out in AML cells. Lower panel: Typical INT-stained colony pictures.

**Figure 2: Serine phosphorylation of the protein orchestrates PHF8 functions in AML.**

**(A)** Colony numbers of human THP1 AML cells transduced with ER-fused PHF8 AA (mimicking non-phosphorylated form) or PHF8 DD (mimicking phosphorylated form) allowing an inducible expression in the presence of 4-OHT. Error bars indicate standard deviation of four independent experiments. Sidak's multiple comparison test (2way ANOVA, **** $p < 0.000$, ns, nonsignificant). Lower panel: Typical INT-stained colonies. **(B)** Number of colonies using equivalent constructs with an additional enzymatic dead F279S mutation. Error bars indicate standard deviation of four independent experiments, 2way ANOVA, nonsignificant ns. Lower panel: Typical INT-stained colonies. **(C)** Proliferation assays, 1.500-2.000 cells were seeded in a 96-well plate and in 100 µl of medium per well. The CellTiter-Glo® luminescent assay kit was used to determine the number of viable cells in culture. **(D)** Bar charts represent percentage of Annexin-V positive cells analyzed by flow cytometry after 4-OHT induction. Pair t-test (* $p < 0.05$). **(E)** Kaplan-Meier curves for disease-free survival of NSG mice transplanted via tail vein injection with 1x10E5 human THP1 cells, after 5 days antibiotic selection, transduced with indicated constructs (n=10 mice per group). Prior to transplantation, mice were conditioned with sublethal radiation (2.5 Gy). Log-rank (Mantel-Cox) Test was used to compare survival curves.

**Figure 3: Epigenetic activity of phosphorylated PHF8 triggers interferon type-I response mediated apoptosis.**

**(A-H)** Deep-proteome quantification analysis of the indicated samples **(A)** Principal component analysis (PCA) of all quantified proteins of the samples in the proteome dataset (a-h, n=4, biological replicates per group). **(B)** Unsupervised hierarchical clustering of differentially regulated proteins between the sample groups as heat map. The color code indicates z-scored log 2 protein intensities of multiple sample t-test (oneway ANOVA, Permutation-based FDR <0.05) significant. **(C)** Significantly enriched gene ontology (GO) terms and pathways. Enrichment analysis (Fisher's exact test) of differentially regulated proteins in each of the sample groups. Regulated proteins were compared to the unchanged proteome in the dataset based on the GO, KEGG, and Keyword terms. **(D)** Network analysis of enriched pathways for proteins significantly upregulated in PHF8 DD cells. The size and color of nodes indicate number of proteins participating in each pathway. The network analysis was performed in Cytoscape version 3.9.1. **(E)** Scatterplot comparing the quantified log 2 protein intensities in PHF8 AA vs PHF8 DD cells (data obtained by fractionation proteome experiment, n=8 fractions per sample). Purple dots indicate proteins participating in response to type-I interferon (GO term). The marked protein names represent significant regulations (permutation-based FDR, 0.05). **(F)** Scatterplot comparing the quantified log 2 protein intensities in PHF8 AA vs PHF8 DD cells (data obtained by fractionation proteome experiment, n=8 fractions per sample). Pink dots indicate proteins related with apoptotic pathways (GO term). The marked protein names represent significant regulations (permutation-based FDR, 0.05). **(G)** Venn diagram showing the number of shared proteins between pathways in response to type-I interferon and apoptosis in PHF8 DD cells (GO term). **(H)** Boxplot representation of selected significantly regulated proteins participating in response to cell-intrinsic immune response and type-I interferon (n=4, biological replicates per group).

**Figure 4: Phospho-PHF8 directly activates key initiators of cell-intrinsic immune response.**

**(A)** Profile plot of PHF8 genome occupancy (ChIP-seq) in THP1 PHF8 AA compared to THP1 PHF8 DD cells. **(B)** Volcano graph depicts all regulated genes in THP1 PHF8 DD cells. Differential expression is represented as LogFC in (X) versus PHF8 ChIP-seq MACS analysis presented as peakScore in (Y). Upregulated genes with significance higher than log 0.5 (>log 0.5) are colored in violet. **(C)** Scatter plot of the highly significantly (>log 0.5) upregulated genes in the transcriptome of PHF8 DD cells (logFC) and PHF8 DD targets resulting from PHF8 ChIP sequencing (peakScore). **(D)** Protein network analysis of the correlation of sixteen highly significantly (>log 0.5) upregulated genes (cell intrinsic immune response inducers) in the transcriptome of PHF8 DD cells and PHF8 DD targets resulting from ChIP sequencing. Pink color represents higher confidence based on experimental evidence. The protein–protein interaction network was established using STRING database and visualized in Cytoscape version 3.9.1. **(E)** ChIP-qPCR analysis of histone mark H3K9me2 on the targeted promoter of the indicated genes in THP1 PHF8 AA and THP1 PHF8 DD cells. ChIP signals are presented as percentage of input. Error bars indicate SD of three independent experiments. Sidak's multiple comparison test (2way ANOVA, **** $p < 0.0001$). **(F)** RT-qPCR time-course analysis (left) of the expression of specified human genes. The relative expression of each gene was independently analyzed in two cell groups: PHF8 AA and PHF8 DD. Each group consisted of non-induced cells and cells induced with tamoxifen (4-OHT). Non-induced samples within each group were used as references for assessing the relative expression of the genes at each time point. Error bars indicate SD of three independent experiments. Bar charts (right) of RT-qPCR analysis at 24 hours after 4-OHT induction. Expression levels are relative only to the PHF8 AA 0mM (4-OHT) cells. Error bars indicate SD of three independent experiments. Tukey's multiple comparison test (2way ANOVA, ** $p < 0.0023$, **** $p < 0.0001$). (**G)** RT-qPCR time-course analysis of the expression of RIG-I and IFN beta human genes. The relative expression of each gene was independently analyzed in two cell groups: PHF8 AA and PHF8 DD. Each group consisted of non-induced cells and cells induced with tamoxifen (4-OHT). Non-induced samples within each group were used as references for assessing the relative expression of the genes at each time point.

Error bars indicate SD of three independent experiments. Tukey's multiple comparison test (2way ANOVA, **** $p < 0.0001$). **(H, I)** ChIP-qPCR analysis of (left) PHF8 or (middle) histone mark H3K9me2 on CMPK2 or IFIT5 targeted promoter in THP1 cells (Control) or THP1 cells after 12 hours of OKA/ATRA treatment. ChIP signals are presented as percentage of input. Error bars indicate SD of three independent experiments. Sidak's multiple comparison test (2way ANOVA, ** $p < 0.023$, *** $p < 0.0009$, **** $p < 0.0001$). RT-qPCR time-course analysis (right) of the expression of CMPK2 or IFIT5. The relative expression of each gene was independently analyzed in non-treated and treated groups of cells. Non-treated samples were used as references for assessing the relative expression of the genes at each time point. Error bars indicate SD of three independent experiments. Tukey's multiple comparison test (2way ANOVA, **** $p < 0.0001$). **(J-K)** Left panels: Bar charts represent normalized colony numbers of human THP1 AML cells co-transduced with non-targeting empty vector control (Control empty) or lenti-CRISPR-V2 guide targeting the indicated endogenous genes (CMPK2 sgRNA 7, CMPK2 sgRNA 9 or IFIT5 sgRNA 1, IFIT5 sgRNA 2) as well as PHF8 vs empty vector (Control) respectively. Non-targeting empty vector control cells were taken as the reference for normalizing the colony numbers in each group. Error bars indicate SD of three independent experiments. Tukey's multiple comparison test (2way ANOVA, ** $p < 0.0033$, *** $p < 0.0007$, nonsignificant ns). Right panels: Representative western blot analyses of the indicated proteins.

**Figure 5: Pharmacological mediated phosphorylation of PHF8 orchestrates cell-intrinsic immune response in human AML.**

**(A)** Barcode plot showing GSEA of ATRA gene signature. **(B)** Bar charts illustrating the impact of ATRA treatment on human AML cells. It displays normalized colony numbers of THP1 cells transduced with empty vector (control) or PHF8 wild type (PHF8) and treated with ATRA (12 hours) at the indicated concentration ($10^{-8}$M). Non-treated cells were taken as the reference for each group. Error bars representative of four independent experiments. Tukey's multiple comparison test (2way ANOVA, * $p < 0.01$, **** $p < 0.0001$). **(C)** Bar charts display normalized percentage of Annexin-V positive cells after flow cytometry analysis. Non-treated cells were taken as the reference for each group. Error bars indicate standard deviation of four independent experiments. Tukey's multiple comparison test (2way ANOVA, * $p < 0.03$, *** $p < 0.0005$, **** $p < 0.0001$). **(D)** Scatter plot showing enriched GO terms of significantly regulated phosphoproteins in THP1 PHF8 cells upon 12 hours ATRA treatment ($10^{-8}$M). Changes of phosphoproteins were compared to the unchanged phosphoproteome in the dataset based on the Gene Ontology, KEGG, and Keyword terms; y-axis shows the negative log of P-value obtained from the Fisher`s exact test. **(E)** Dot plot showing changes in phosphosites of displayed proteins (12 hours ATRA) in THP1 cells transduced with empty vector (EV) or PHF8 (PHF8). Red color and asterisk highlight specific IFIT5 targets. (ANOVA test Permutation-based FDR < 0.05). Sizes and colors of the dots are proportional to the averaged phosphosite intensity, *z*-scored ($log_2$ intensity), (n=4, biological replicates per group). **(F)** Representative western blot analyses of time-course experiments (n=3) following treatment with indicated ATRA concentration. Actin was used as a loading control for total extract, Lamin B1 for nuclear extract of THP1 cells expressing PHF8. **(G)** Western blot analysis of NF-κB (p65) protein levels (12 hours of ATRA) in nuclear (Lamin B1 loading control) and cytosolic (tubulin loading control) extracts of THP1 cells (n=3). Cells were transduced with empty vector (Control) or PHF8 wt (PHF8). **(H)** Phosphoproteome map of early interferon type-I response and apoptosis in PHF8 AML cells after ATRA stimulation. Significantly regulated phosphoresidues are depicted on proteins participating in the process (n=4, biological replicates per group, one way ANOVA, Permutation-based FDR < 0.05). Arrows indicate protein-protein interactions and phosphorylation events curated from experimentally defined databases. S-serine,

T-Threonine, Y-Tyrosine.

**Figure 6: PHF8/IFN type-I response protein signature is frequent in AML patients and provides novel opportunities for future targeted therapies.**

**(A)** Unsupervised hierarchical clustering of AML patient samples (n=204 samples) based on proteins participating in gene ontology term interferon type-I mediated signaling pathway. The clustering identifies two major sample groups (Group-1 and Group-2) as highlighted in heat map. Annotations at the top of the heat map show patient disease status and PHF8 protein expression. **(B)** Box plot showing the differential expression of PHF8 in AML samples based on interferon protein expression cluster (Group-1=102 patient samples vs Group-2=102 patient samples). Two sample t-test, permutation-based FDR <0.05 represented as significant. **(C)** Dot plot for PHF8 expression versus PC2 scores of 204 AML patient samples (n=177 primary and n= 27 relapsed AML) based on the IFN-I signature subproteome. **(D)** Immunoblot analysis of total PHF8 levels of nine AML patient samples (P1- P9). Actin was used as loading control. **(E)** Immunoprecipitated PHF8 from primary AML patient cells expressing high PHF8 levels, untreated (Control) or under combinatorial treatment with OKA/ATRA (O/A) and immunoblotted for phospho-Ser (upper panel) as well as for total PHF8 protein after membrane stripping (lower panel). **(F)** Violin plot depicting total numbers of colonies of five primary AML patient samples with high expression of PHF8 (n=5). Significance was tested using Tukey's multiple comparison test (2-way ANOVA, * $p < 0.02$) ** $p < 0.008$, *** $p < 0.0002$, **(G)** AML patient samples with low expression of PHF8 (n=4), treated with the indicated concentrations of ATRA, OKA (OKA 20 minutes incubation). Tukey's multiple comparison test nonsignificant ns. **(H-I)** Colony morphology of primary human AML patient cells expressing high (H) or low (I) PHF8 levels. Cells were treated with ATRA ($10^{-8}$M) or/and OKA (500nM OKA, 20 minutes incubation).

Figure 1

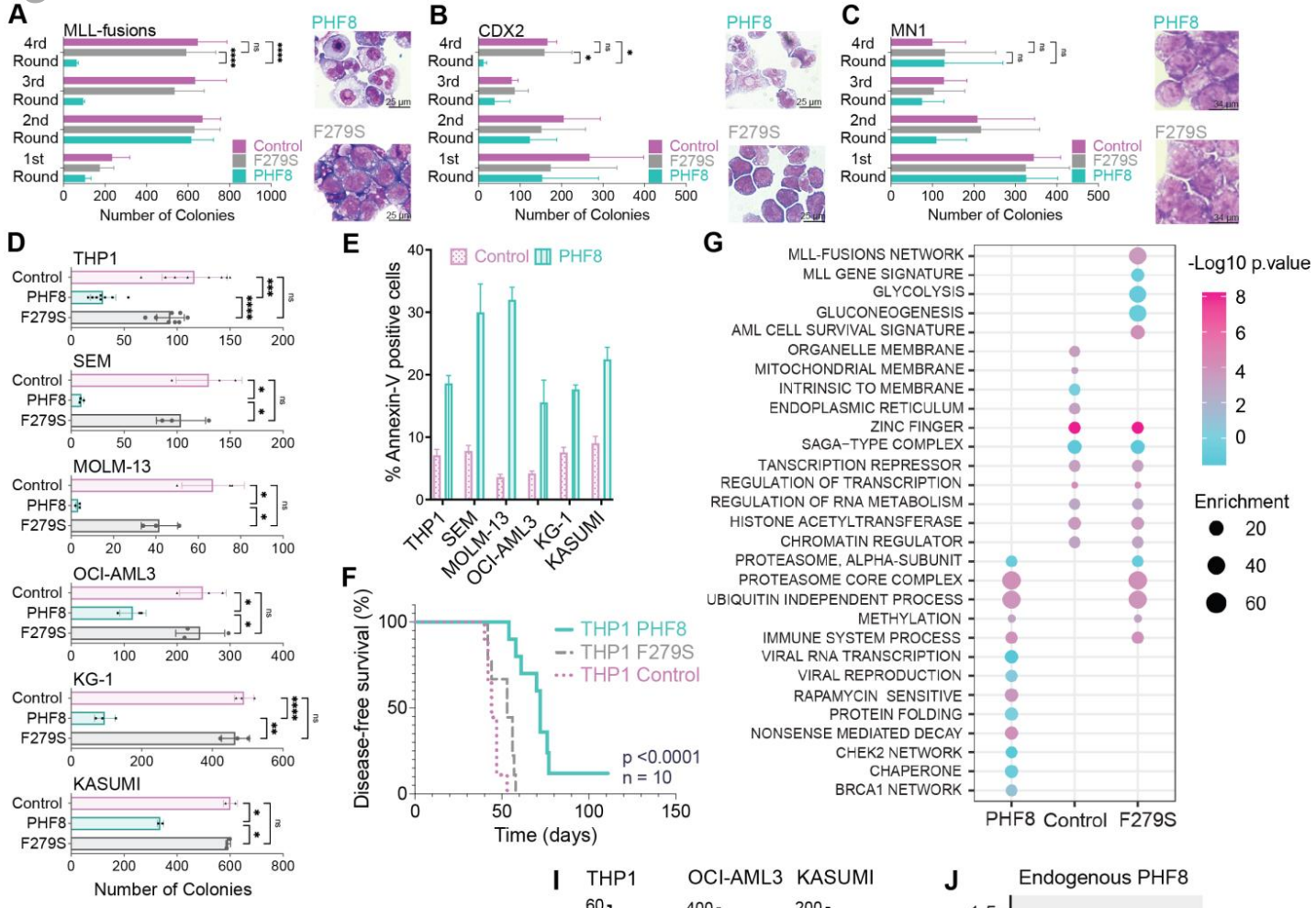

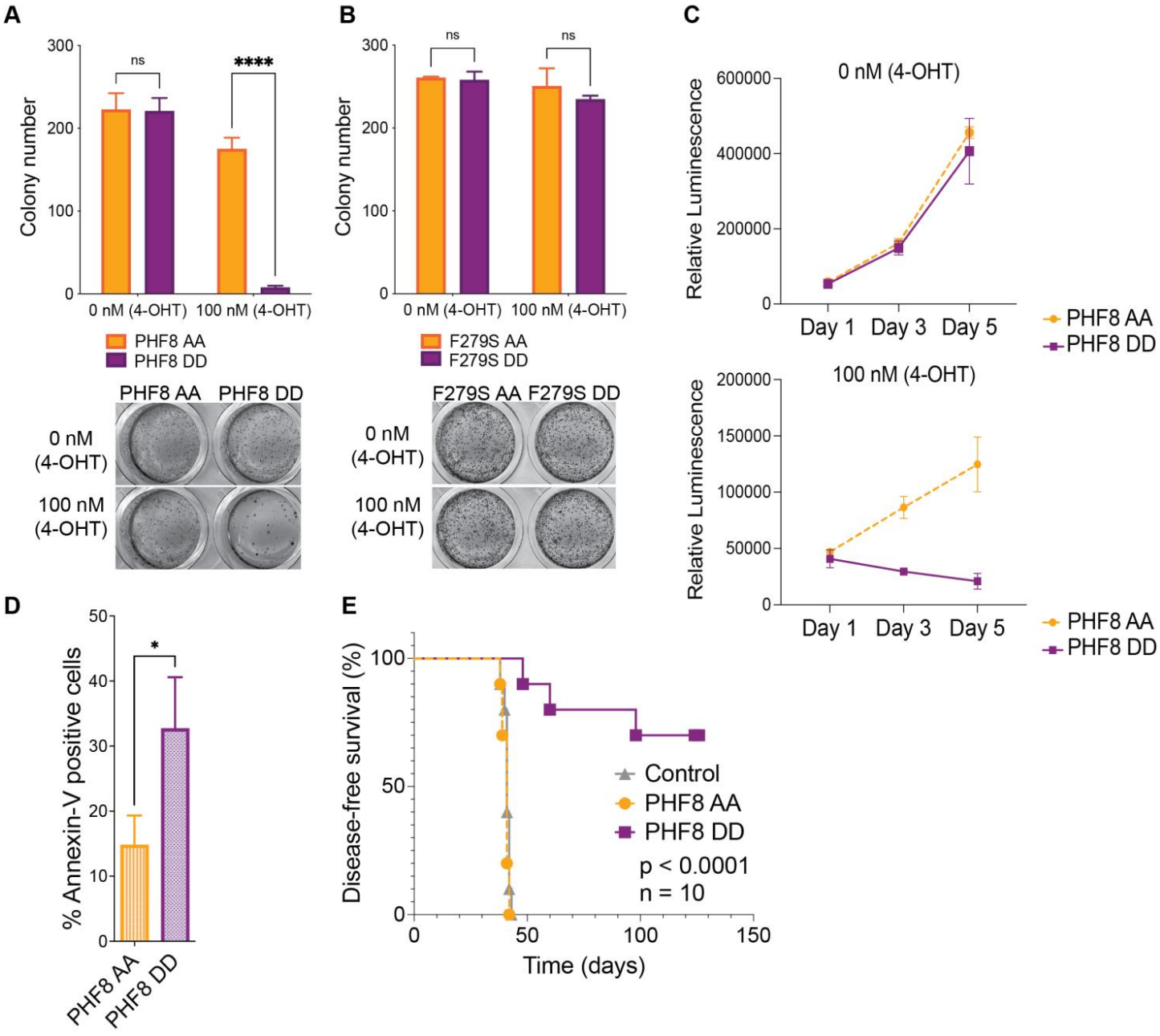

# Figure 3

Figure 3

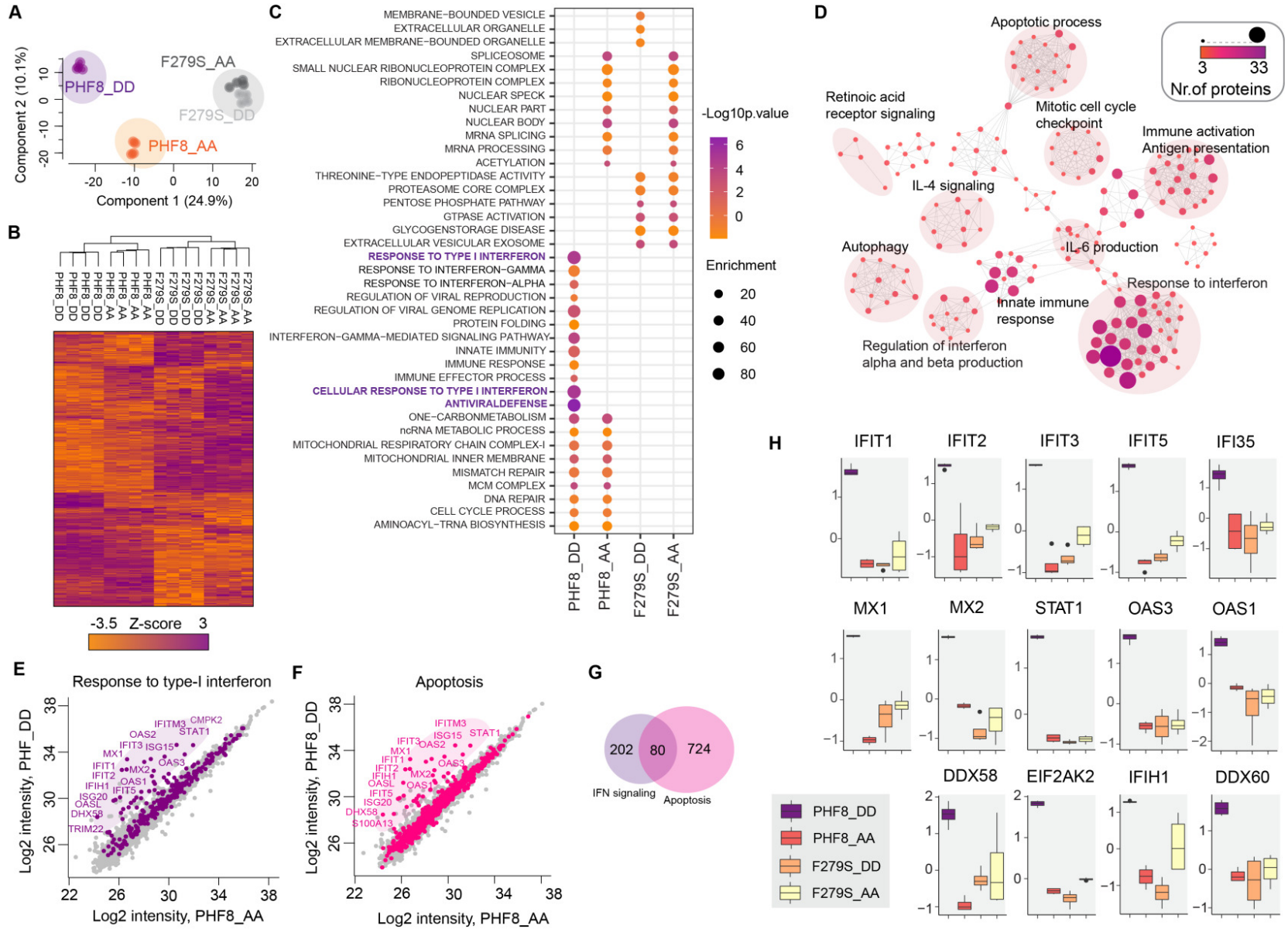

**Figure 4**

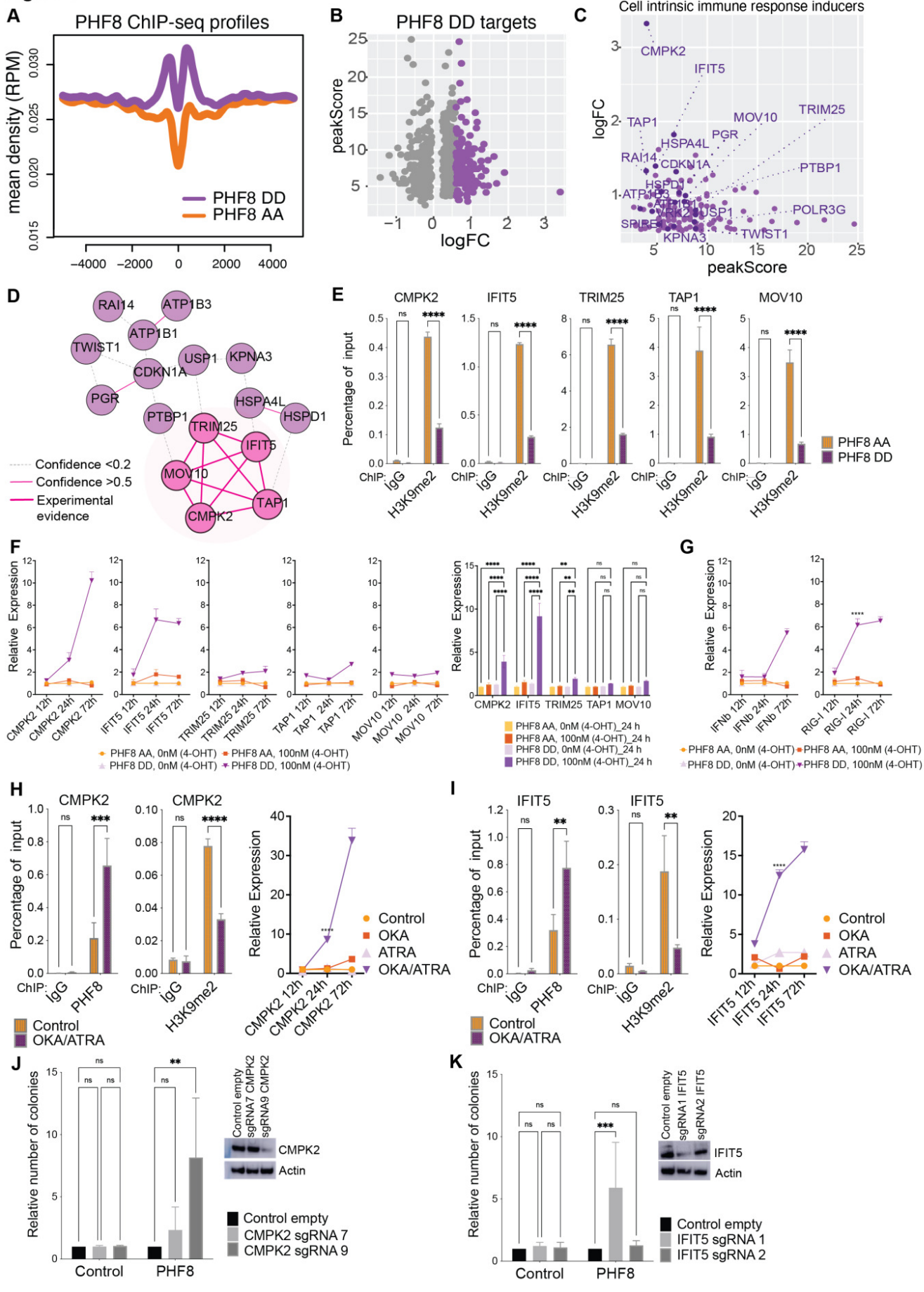

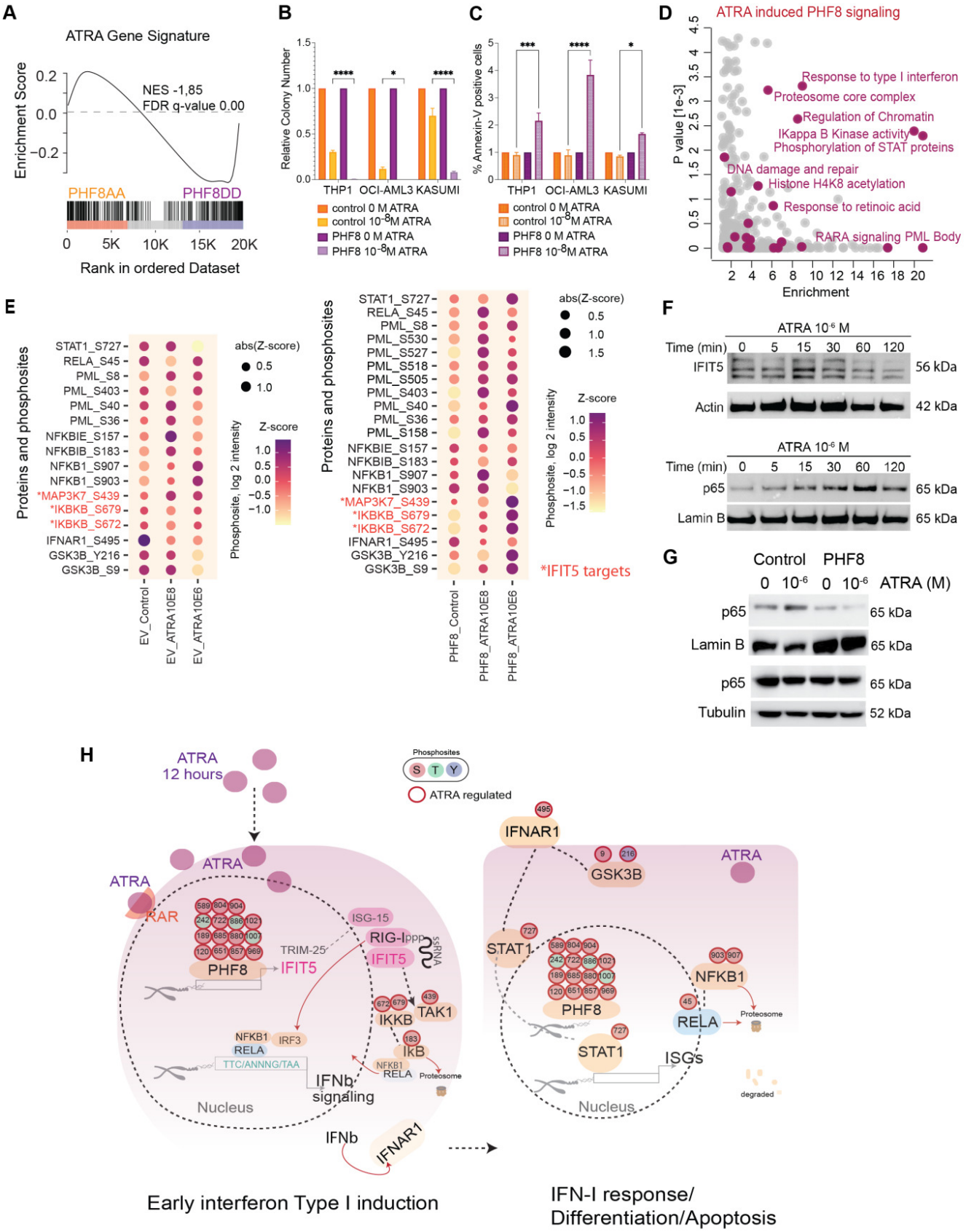

**Figure 6**

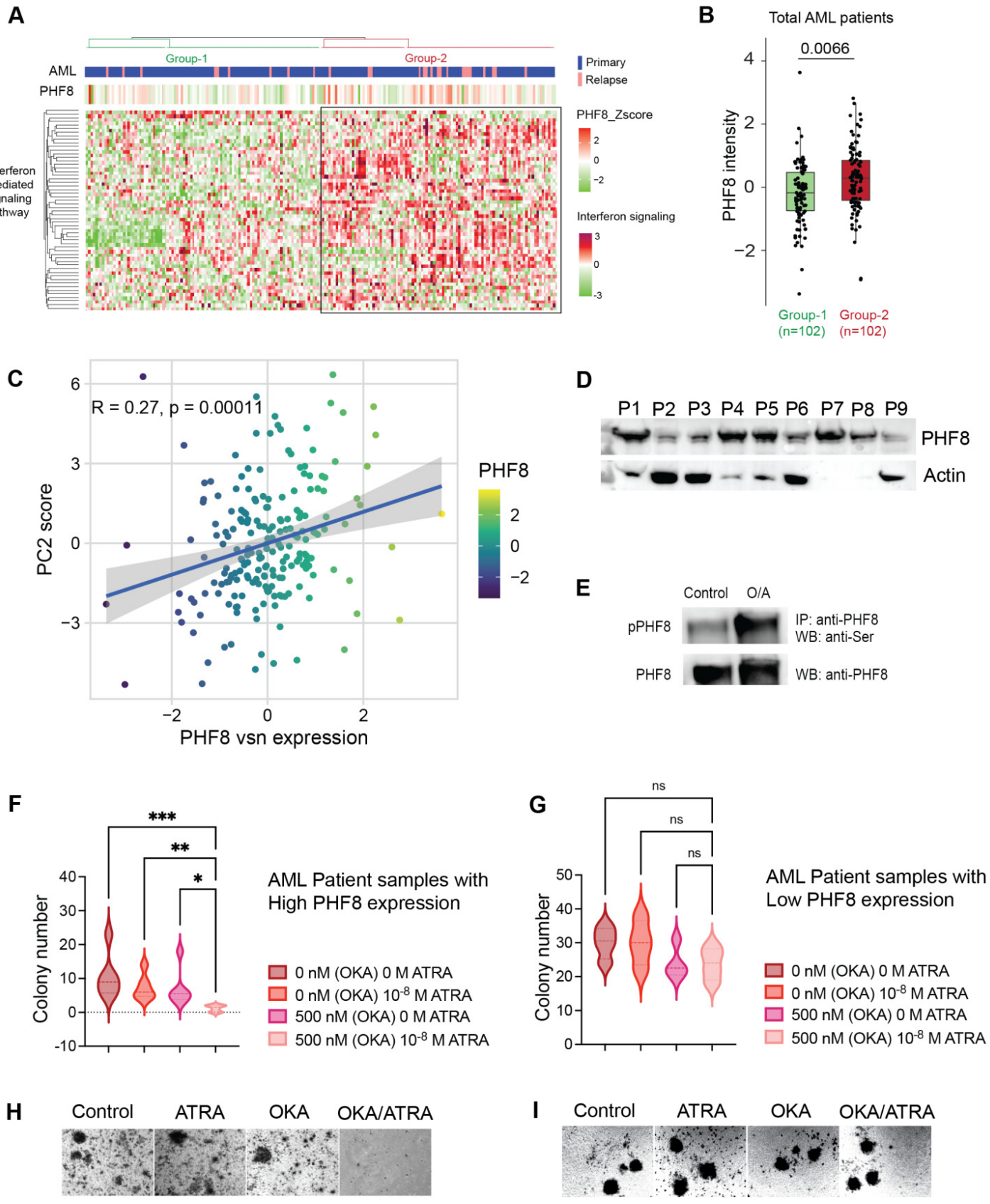

# The Dynamic Epigenetic Activity of PHF8 Coordinates Cell-intrinsic Immune Response Inducing Cell Death in AML

**Pharmacologically induced PHF8 phosphorylation activates RNA sensors triggering IFN-I response and provides a novel avenue for AML immunotherapy.**

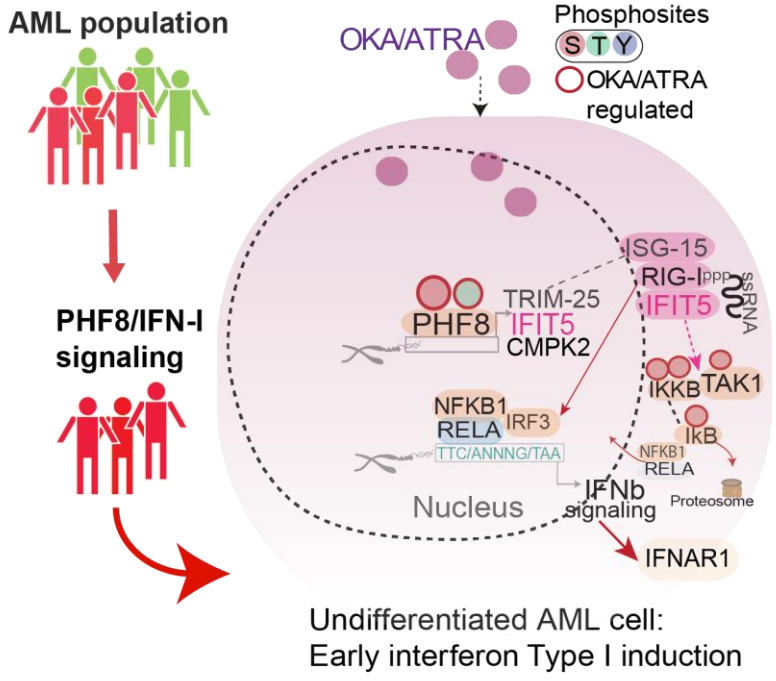


**The histone demethylase PHF8 is a master regulator of cell-intrinsic immune response, activating interferon stimulated genes followed by apoptosis in AML.**

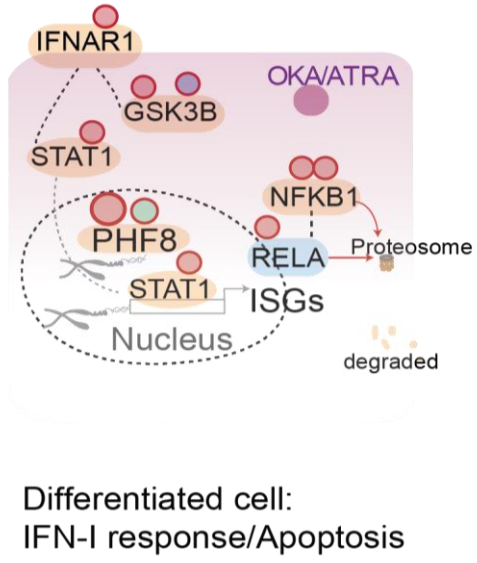


**Pharmacological support of PHF8 phosphorylation induces cell-intrinsic immune response that significantly impairs growth of Acute myeloid leukemia. These findings provide novel opportunities for immunotherapeutic strategies against AML. Felipe-Fumero E. et al, DOI**